Utilization of a curved focal surface array in a 3.5m wide field of view telescope

Lt. Col. Travis Blake
Defense Advanced Research Projects Agency, Tactical Technology Office
E. Pearce, J. A. Gregory, A. Smith, R. Lambour, R. Shah, D. Woods, W. Faccenda
Massachusetts Institute of Technology, Lincoln Laboratory
S. Sundbeck
Schafer Corporation TMD
M. Bolden
CENTRA Technology, Inc.

ABSTRACT

Wide field of view optical telescopes have a range of uses for both astronomical and space-surveillance purposes. In designing these systems, a number of factors must be taken into account and design trades accomplished to best balance the performance and cost constraints of the system. One design trade that has been discussed over the past decade is the curving of the digital focal surface array to meet the field curvature versus using optical elements to flatten the field curvature for a more traditional focal plane array. For the Defense Advanced Research Projects Agency (DARPA) 3.5-m Space Surveillance Telescope (SST)), the choice was made to curve the array to best satisfy the stressing telescope performance parameters, along with programmatic challenges. The results of this design choice led to a system that meets all of the initial program goals and dramatically improves the nation's space surveillance capabilities. This paper will discuss the implementation of the curved focal-surface array, the performance achieved by the array, and the cost level-of-effort difference between the curved array versus a typical flat one.

1. INTRODUCTION

Curved-detector technology for applications in astronomy, remote sensing, and, more recently, medical imaging has been a component in the decision-making process for fielded systems and products in these and other various disciplines for many decades. The use of large film negatives on early-to-mid 20th century Paul-Baker telescopes was seen as a natural choice, given the large field curvature retained in those early designs. However, as digital, silicon-based camera technologies took over, the choice to use curved, instead of more easily manufactured flat detectors, became difficult and often controversial. This foreboding occurs because of the perceived added handling and fragility to an already delicate scientific or commercial instrument. Furthermore, early attempts achieved poor noise performance and surface figures of merit that exceed program technical specifications. Existing optical designs, on the other hand, *flattened* the light that was gathered by an optical imaging system onto planar detectors. Such detectors were inexpensive, easy to manufacture, and possessed sufficiently good noise performance for the desired applications.

Optical system designs, however, have increased in complexity as the demands of data-intensive communities like astronomy and Earth-imaging services changed. In the instance of the astronomy and space surveillance domains, the scientific and technical drivers of new-start efforts required telescope systems possessing sufficient detection sensitivity to find faint (small and/or distant) targets over large fields-of-view with rapid cadence and excellent image quality. Existing large-aperture, wide field-of-view systems such as Pan-STARRS and the Space Surveillance Telescope, as well as planned telescopes such as TMT, GMT, and LSST incorporate a number of design decisions that achieve some or all of these choices. Astronomical systems, broadly speaking, require a combination of detection sensitivity to detect both point sources and wide-area surface brightness. These tend to drive camera systems towards small pixels and large-aperture telescopes. Down-looking remote-sensing systems need to minimize optical distortion on space-based platforms in order to maintain ground sample distance needs. Space surveillance telescopes, both ground and space-based, are largely detection systems that require optimum detection sensitivity.

In all these applications, a cost-value trade must be made among aspects of system performance (e.g. throughput, weight, step-and-settle) and complexity of component technologies. Many previous efforts to *simplify* component design hinge on reducing the number of refractive elements in any optical design. Refractive elements are known for introducing chromatic aberration, but also are responsible for causing field-dependent coma, vignetting, and illumination loss [1,2,3]. Additional efforts are needed to co-align optical elements, introducing additional degrees of freedom and undesirable caustics when fielding systems. For space systems, there is an added benefit that removing refractive elements reduces mass budgets.

Refractive elements, however, in traditional optical designs such as Cassegrain and Richey-Chretien telescopes are necessary to eliminate the Petzval field curvature produced by the reflective elements. One solution is to *curve* the imagers to match the inherent field curvature produced by reflective elements. This, as one might imagine, presents challenges for silicon-based devices and their component circuitry; CCDs have been perceived as too fragile to handle. But despite this perception, efforts at matching the Petzval field curvature by altering the camera construction have been pursued.

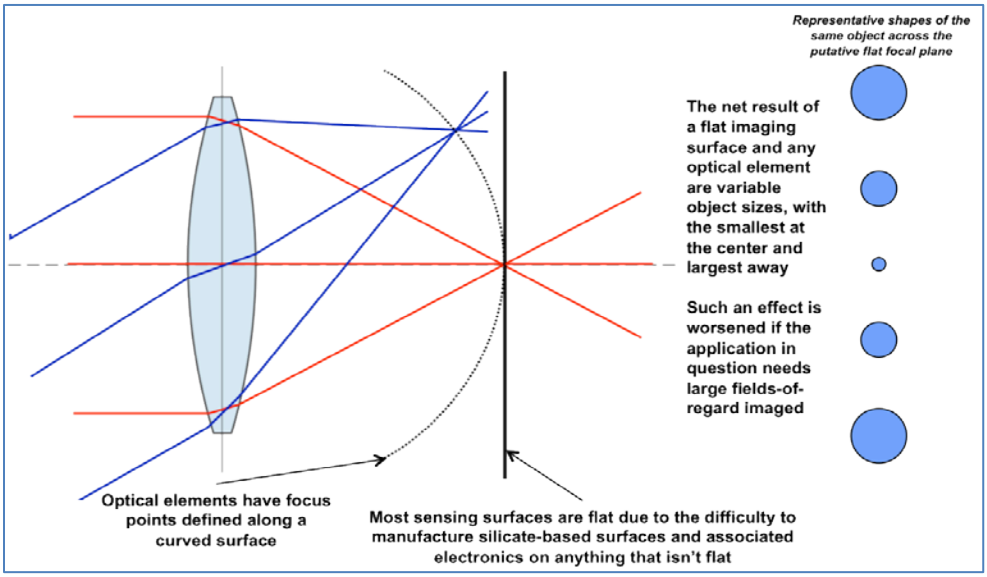

Fig. 1: Impact of inherent Petzval curvature on focused light on a flat detector. Bigger spots lead to lower signal-to-noise ratio, reducing the sensitivity of the instrument. To compensate, one must choose a smaller field-of-regard for the sensor or adopt a curved focal plane.

The Kepler Space Telescope used a nearest-curvature solution to tile its ~13° diameter FOV. Kepler, designed to detect Earth size planets in the "habitable zone" orbiting $9<m_V<16$, F through M type stars, employed a 0.95-m aperture Schmidt telescope to illuminate the 96-megapixel focal plane. The camera contains twenty-one Science CCD modules, each consisting of two CCD 2k×4k imagers aligned tangentially to the local field curvature surface. A local field flattener works to remove any remaining curvature. Though advantageous in limiting the size of field flatteners, it still included large gaps of ~< 0.5 degrees. For applications requiring better fill factors, in particular for sky-survey programs like SST, low fill factors would defeat the purpose of attempting to match the field curvature.

2. SST enabled by curved WFC

As mentioned earlier, the SST design was optimized for detection sensitivity while retaining a large field-of-view and rapid step-and-settle. The purpose was to find, fix, and track small (<20-cm)) objects at the distance of the geosynchronous belt, observed from a relatively high elevation site on Earth. Detection sensitivity is strongly affected by mirror diameter, as well as CCD noise parameters and sky conditions. An early trade in the SST program was to choose a primary-mirror size that could be manufactured, polished, coated, and transported by truck. These somewhat subjective constraints restrict mirror diameters to below 4 meters.

Because of the desire to obtain as large a uniformly illuminated field-of-view as possible, SST used a derivative of the three-mirror Mersenne-Schmidt. This mirror design affords the opportunity to retain the inherent Petzval field

curvature or use a series of elements to flatten the scene. As mentioned earlier, the latter would lead to vignetting, a non-uniform point response functions across the FOV, and reduction in the search area. By using curved CCDs, MIT LL achieved a sizeable 6-square-degree FOV with relatively small 15-µm pixels with only ≲10" gaps between the 12 discrete CCDs. Additionally, the choice of using the compact Mersenne-Schmidt and retaining the field curvature allowed for a relatively compact design that supports rapid step-and-settle.

3. MANUFACTURING

Achieving the curved wide-field camera (WFC) incorporates two major steps: (1) curving of individual back-illuminated (BI) CCD imagers with little or no change in the performance characteristics and (2) alignment of 12 imagers to achieve the large field-of-regard desired for SST.
Three components of the CCD imager are altered in order to achieve the desired curvature: the sensing layer, its associated etched circuitry, and a carrier silicon wafer. The sensing layer is a back-illuminated CCD: that is, the actual structure of the CCD that collects photoelectrons is buried within the silicon layer that receives the incoming photon flux. MIT LL innovated three significant mechanical processes in order to make the curved CCDs:

1. Thinning both the illuminated silicon surface and its supporting substrate to make flexible imager wafers. This process will be referred to as Double-Flush Thinning (DFT).
2. Bonding fixturing to align the image wafers on to the curved silicon mandrel and to eliminate cocking or slippage after application of the epoxy
3. Vacuum chuck curing to ensure that the epoxy bonding was strong enough to resist large temperature swings.

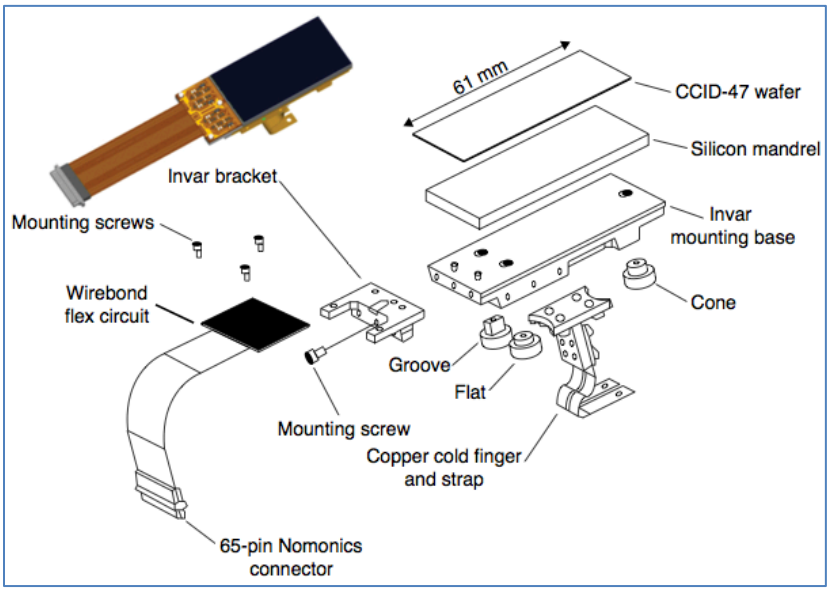

Fig. 2: Breakout of individual CCID-47 imagers. The light-sensing surface or wafer has been thinned by the Double-Flush method and bonded to a machined silicon mandrel. Thermal variations are minimized by using Invar alloy components, which has a very good expansion coefficient match to silicon. A copper cold strap provides heat removal through a special mounting in the Dewar interior. The flexprints connect down to the analog electronics that are responsible for "counting" the photons.

Double flush-thinning
The DFT process provides imagers with sufficient flexibility to be mounted to a curved silicon mandrel. In principal, this process is a continuation of back-illumination methods routinely performed by the imager laboratory at MIT LL. The BI process has been described in detail previously [4,5], and is presented briefly below. A finished front-illuminated CCD is inverted on a carrier and the single-crystal Si backside is etched in an acid solution to a thickness ~45-µm. The resulting backside is passivated with a boron implant and laser anneal, leaving a surface with high quantum efficiency through the visible and beyond 900-nm wavelength (reaching about 50% at 950 nm). Due

to the very high resistivity of the CCD Si and the imposed clock biases, the electric field extends through the 45-µm layer. This yields a nearly 100% collection efficiency of photoelectrons (as shown in Fig. 3a).

At that point, the devices were ready for the DFT process, where the illuminated surface was mounted temporarily to a second carrier wafer (Fig. 3c) and the first carrier wafer was thinned to about 150-µm. (Fig. 3d). The second carrier was released, leaving a device about 200-µm thick overall, as shown Fig. 3e, and that could be diced for individual CCD mounting. This structure was a good compromise between strength and flexibility, allowing the CCDs to be deformed to the 5.44-m radius with over 95% yields. (Fig. 3f).

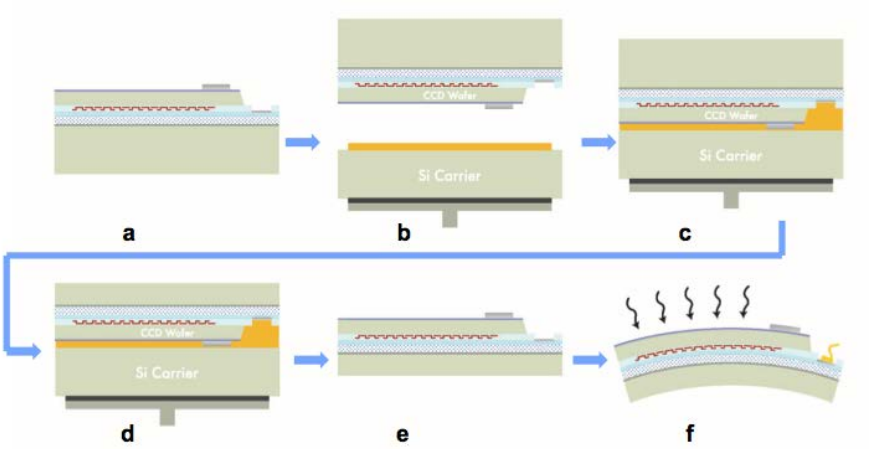

Fig. 3: Back-illumination detail150-mm bondpads of the DFT process, resulting in an approximately 200-µm thick Si structure, capable of being bent to the appropriate radius.

Alignment of imager onto silicon mandrel
Silicon mandrels, on which the CCID47's were mounted, were machined commercially to have surface accuracies better than 3 µm. A double-flush thinned imager was secured to each using an epoxy.

The choice of epoxy
Epoxy testing required several candidates to ensure uniformity of coverage; that no air-gaps occurred; and that strong bonding persisted over a large range (-100°C to 50°C) of expected operational temperatures. Despite the presence of commercial products and data sheets, MIT LL performed bench tests against a dozen epoxies to demonstrate bonding strength against temperature and mechanical deformations. The final choice was 301-2, supplied by EpoTek.

The mounting fixture
MIT LL developed an in-house solution to ensure minimal cocking of the imaging surface to the silicon mandrel. Two turndown screws were used to maintain well-machined aluminum plates parallel to the desired mounting direction.

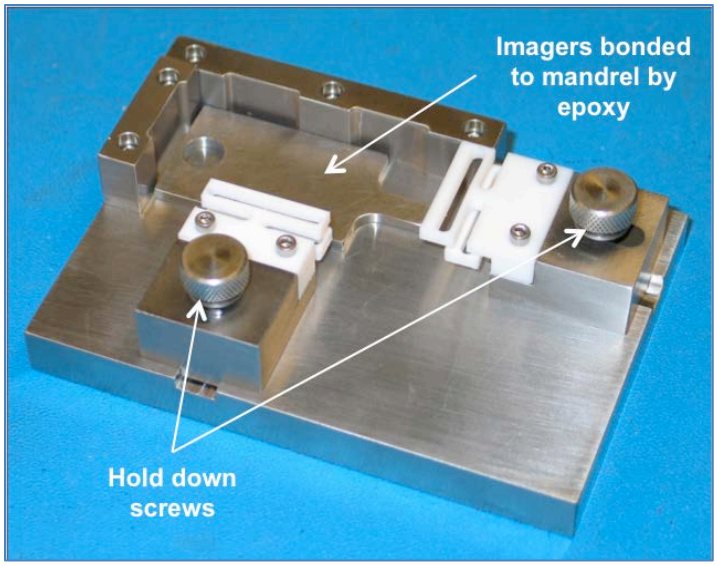

Fig. 4: Two-axis precision mounting tools ensure that imager surface and mandrel are well mated. This ensures that no cocking is introduced when final camera integration of the 12 CCDs is performed.

Vacuum chuck bonding

MIT/LL incorporated a novel vacuum method to enhance the bonding of the imagers to the mandrel carrier wafers. A porous ceramic surface, capable of being milled to the desired figure, was connected to a vacuum source. A protective layer of porous Teflon foil was placed on the concave, milled portion to protect the illuminated surface of the wafer being bonded to the silicon mandrel carrier. The vacuum was drawn through the chuck to allow the mandrel and silicon to be brought together with a large, but non-destructive, force. This vacuum was maintained for up to 7 days to ensure proper curing of the epoxy between the imager and the mandrel.

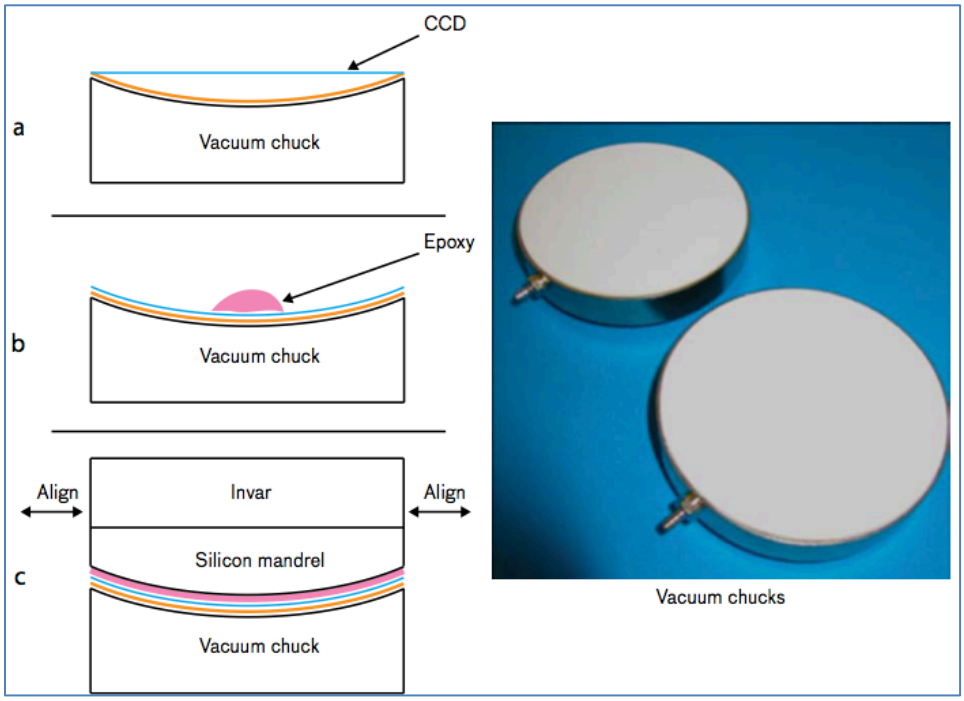

Fig. 5: Custom designed semi-porous ceramic. A multi-day curing process ensures surface stability down to -70°C.

In general, incorporating a number of CCDs into a camera required a suite of quality control testing. MIT LL chose high quality imagers based on the following criteria:

- Surface conformance to R_0=5.44 mm
- Low readout noise
- Low dark current
- Fewer number of bad pixels or columns
- Ability to be electrically paired in the array, as defined by the parallel voltage clock ranges

Once candidate imagers were chosen, they needed to be aligned to each other.

Imager alignment into the packaged camera

Twelve imagers that passed numerous quality control tests were incorporated into the camera. This incorporation required a precise and accurate alignment of the 12 imagers to a radius of curvature of 5.44 mm. The process achieved alignment of 12 high-quality imagers to the desired radius of curvature 5.44 m to an RMS non-conformance of ~6 µm.

A crucial factor in building up the mosaic focal plane of the WFC was incorporating the base mounting plate and a coordinate system that ensured close alignment to the optical axis of the mirrors in SST. The process used known fiducial marks – G10 screws and mounting brackets – found along the face of the mounting plate to define a coordinate system (X", Y", Z"). These values were transformed through a series of rotations and translations to the coordinate frame of the measurements, (X, Y, Z) from the metrology station itself.

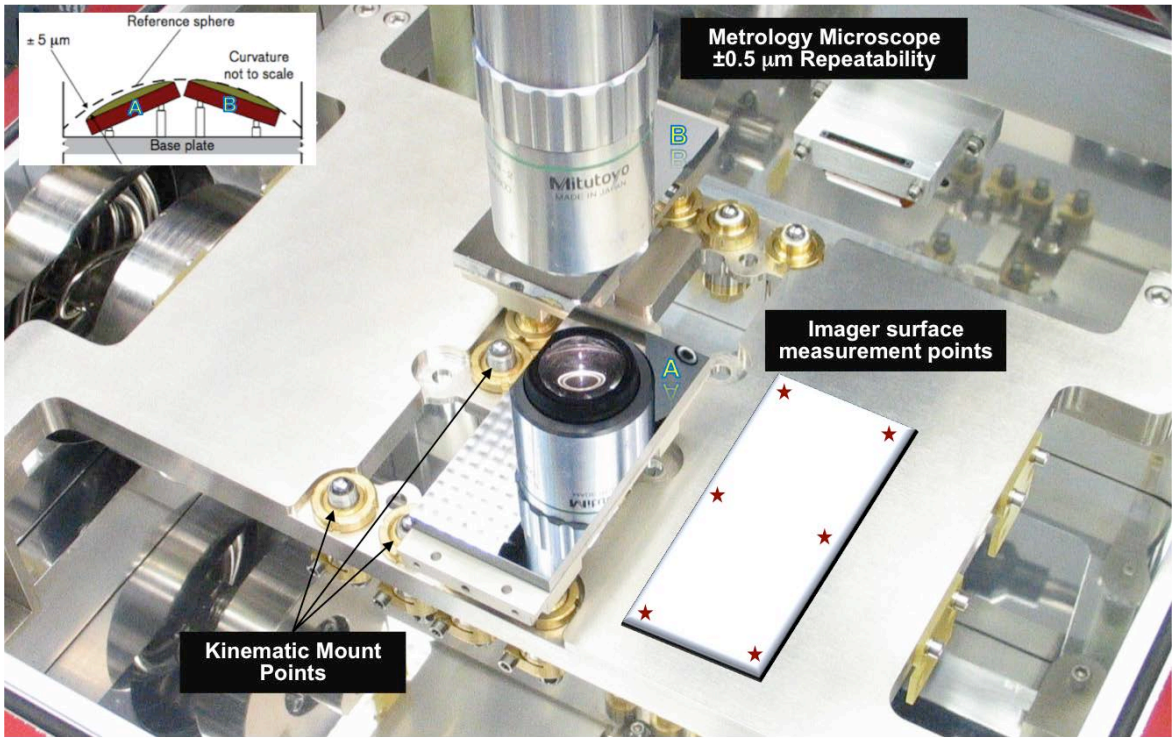

Fig. 6: Metrology measurement station with two of 12 imagers during early alignment. This device provided 3D measurements of the individual CCD surfaces, as well as known fiducial markers on the mounting plate below the kinematic balls. This provided a repeatable, stable reference from which to define a focal surface vertex *perpendicular* to the center of the array and ensured close alignment with the optical axis of the incoming light.

Next, an iterative alignment process on the central four imagers aligned them with the fiducial marks, as a surrogate to aligning them to the optical axis of the mirrors. The 6 positions on each of the 4 central imagers were fit, via a non-linear least-squares algorithm, to a best-fit sphere in the "double-primed" coordinate frame. The Z-height variations were used then to determine the heights of the imagers to achieve a radius of curvature among CCDs of 5.44 m, relative to the base plate. The difference between the measured and desired heights was translated into

relative adjustments of the CCDs. Aluminum shims were cut with a 2-µm precision and placed them between the mounting kinematic ball and the base mount to make the relative height adjustments. The process was repeated until alignment better than 6 µm was achieved.

The flanking imagers were next aligned to the surface defined by the central four. This was again repeated until alignment better than 6 µm was achieved. Both a non-linear least squares fit and a method outlined by G. Luppino (priv. comm 2003) provided numerical verification of alignment.

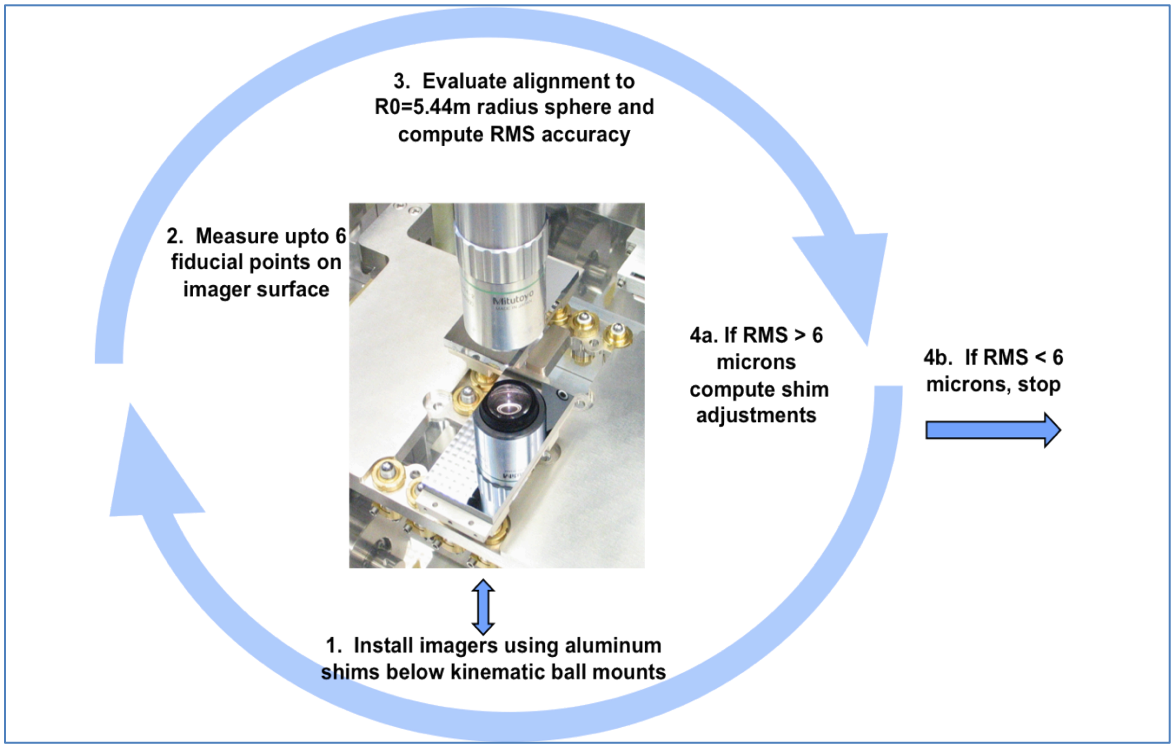

Fig. 7: Overview of iterative process to align imagers.

4. CAPABILITIES ASSESSMENT

Laboratory Dark Current and CTE measurements
Both the dark current and charge transfer efficiency fell within expected ranges for CCDs with a heritage of large well depths and high gain (i.e. produce many DN counts for each photon in order to detect fainter objects). Although, in theory, straining Si decreases the band gap and, thus increases the dark current, the values measured in the laboratory testing of flight components indicated no differences from traditional flat devices..

Field Measurements
Regular observations with the camera indicate that performance has not been sacrificed by curving the imagers. MIT LL based the SST program on a full system model to perform synoptic search of the sky for satellites. This model incorporates the relevant features of camera noise that affect the detection capability of objects in the night sky. The agreement between the model predictions and observed sensitivity against stars is excellent.

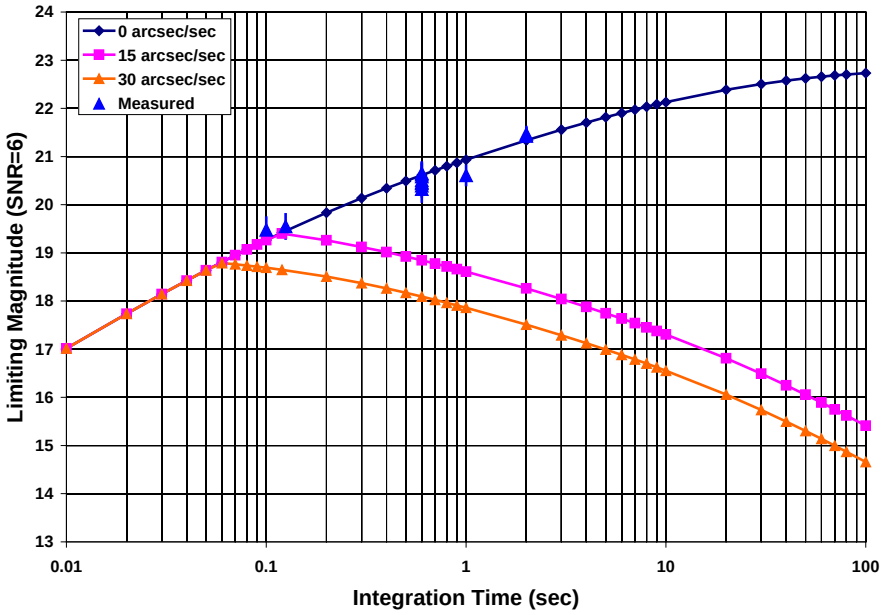

Fig. 8: SST performance model against measured values. Three curves are provided that show the impact of moving targets on sensitivity. The error bars are estimated over several hundred frames per integration time.

Additionally, Woods et al (2013) found a well behaved and relatively uniform point-spread function (PSF) and illumination pattern across the full extent of the camera. Fig. 9 shows the variation in spot size across the field of view. Other than the chips in the upper left corner, the expected pattern of radial symmetry and uniformity is observed. (MIT LL postulates that the chips in the upper left corner are affected by misalignment relative to the focal surface due to thermal variations since camera integration.)

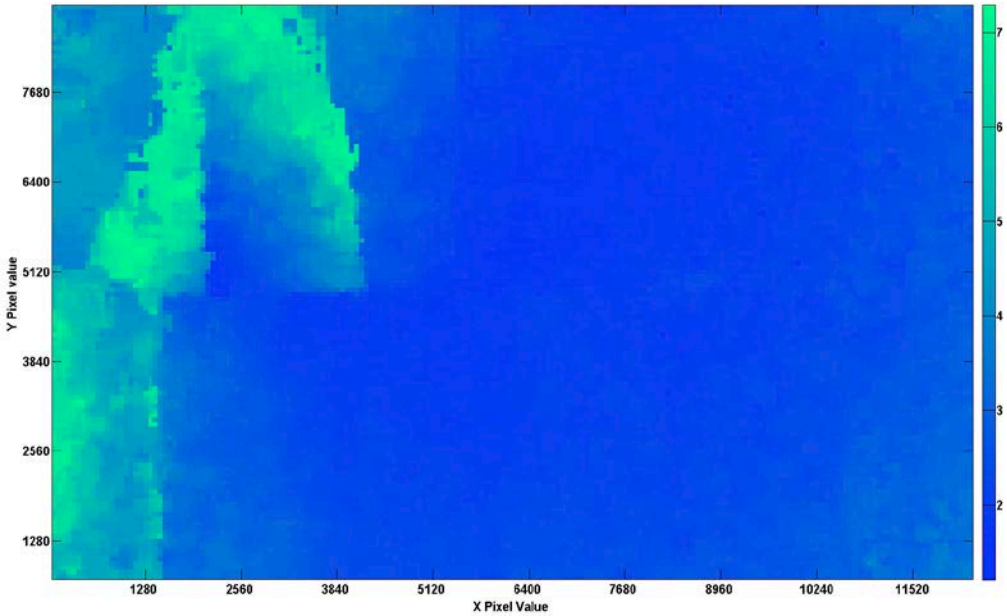

Fig. 9: Spot size across the focal surface from Woods et al (2013). Each data point contains the mean spot size in kernel the size of at least 21 measured FWHMs. averaged over 5 frames of observations. The two chips in the upper left corner appear to be affected by chip alignment relative to the focal plane. The remainder of the focal plane displays the expected radial symmetry that is consistent with optimal mirror alignment[4].

The SST focus and alignment program includes regular analysis of defocused stars to measure aberrations and provide a model for focusing during operations[4]. These analyses find a fairly flat distribution for coma and defocus Seidel aberrations (Fig. 10). This is consistent for a system with a well aligned reflective mirrors and camera. Additionally, the astigmatism and spherical aberration terms that would be present due to a three-mirror design are also uniformly distributed. The total resultant spot FWHM on high quality nights approaches the model predictions for ~1" seeing, under dry conditions.

5. CCD-PROCESSING DIFFERENCES

The extra processing for DFT added about 5% to the total fabrication time of the BI CCDs, and the associated yield loss with the process was 5% or less.

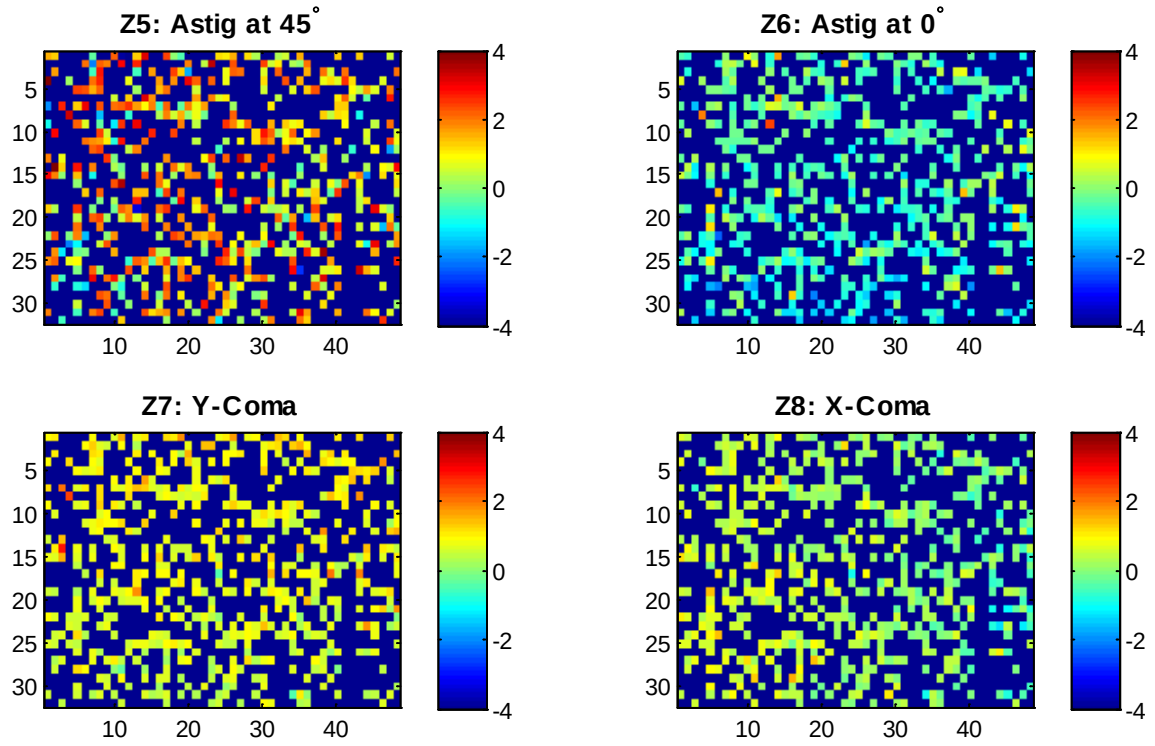

Fig. 10: The Zernike aberration terms are measured for a set of defocused images using algorithms based on associated yield loss with the DONUT software[5]. The pattern of aberration values across the focal plane is fairly uniform, except for slight evidence of a bulk tilt of the tertiary mirror that is manifest by the large-scale gradients in the Z6 and Z8 terms.

6. SUMMARY

SST has paved the way for curved focal plane technology applications in the space surveillance and astronomy domains. DARPA and MIT LL are actively using the curved WFC on SST to observe and track satellites, asteroids, and transient astronomical phenomena for research purposes. SST's novel optical design is enabled by the curved WFC.

The initial cost to build a curved focal surface camera was ~25% more than an equivalent planar focal plane camera. The additional cost includes necessary NRE tooling. The extra processing required for double flush thinning added ~5% to total fabrication time, with ~5% reduction in yield. In the future, producing additional curved arrays are on

the order of 10% more expensive than the equivalent flat array. This cost may be recouped through reduction of the rest of the optical-mechanical design and the cost to operate and maintain is identical.

The surface non-conformance of both the imager and the silicon mandrel to a radius of curvature of 5.44 m is <3 μm. This means that the uniformity of individual imagers is better than 1 part in 1 million. The imager thinning process retains the primary qualities of the imager, including readout noise and dark current.

7. REFERENCES

1. Iwert,O., Ouellette,D., Lesser,M., Delabre,B., *First results from a novel curving process for large area scientific imagers*, SPIE 8453-68, 2012
2. Swain,P., Channin,D., Taylor,G., Lipp,S., Mark,D., *Curved CCD's and Their Application with Astronomical Telescopes and Stereo Panoramic Cameras, Optical and Infrared Detectors for Astronomy*, Proc. of SPIE Vol. 5499, SPIE, Bellingham, WA, 2004
3. Dinyari,R., Rim,S.B., Huang,K., Catrysse,P.B., and Peumans,P.,*Curving monolithic silicon for nonplanar focal plane array applications*, Appl. Phys. Lett. 92, 091114, 2008
4. Woods,D.F., Shah,R.Y., Johnson,J.A., Szabo,A., Pearce,E.C., Lambour,R.L., Faccenda,W.J., *Space Surveillance Telescope: focus and alignment of a three mirror telescope*, Opt. Eng. 52 (5), 053604, May 07, 2013
5. Tokovinin,A., Heathcote,S., *Donut: measuring optical aberrations from a single extra-focal image*, PASP, V. 118, pp. 1165-1175, 2006